148

NASA TECHNICAL MEMORANDUM

NASA TM X-71496

NASA TM X-71496

DIFFUSIVE IGNITION AND COMBUSTION IN A WALL JET

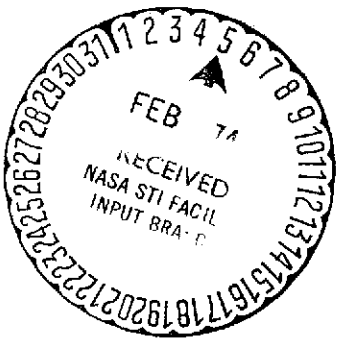

by A. P. Kurkov and R. E. Gaugler
Lewis Research Center
Cleveland, Ohio 44135

TECHNICAL PAPER proposed for presentation at
Symposium on the Fluid Mechanics of Combustion
sponsored by the American Society of Mechanical Engineers
Montreal, Canada, May 13-16, 1974

DIFFUSIVE IGNITION AND COMBUSTION IN A WALL JET

A. P. Kurkov[1] and R. E. Gaugler[1]

Lewis Research Center
National Aeronautics and Space Administration
Cleveland, Ohio

E-7813

ABSTRACT

Hydrogen is injected from a downstream facing step in a wall into a high-temperature stream. Temperature and hydroxyl radical concentration are measured downstream of the injection plane by means of ultraviolet absorption spectroscopy. The experimental results are compared with theory which is based on a finite-difference solution of boundary-layer equations. Finite-rate kinetics equations are included in the analysis. The analytic predictions are also compared with previously obtained experimental results which are based on probe measurements. Comparison is made between calculated and observed ignition distances.

NOMENCLATURE

A,B,C,D	different chemical species
$\overline{A}$	pre-exponential constant in the rate expression
[A]	mole fraction of A
C_p	specific heat
E	activation energy
f	reaction rate
H	total enthalpy
h	static enthalpy
k	specie number
ℓ	reaction number
M	third body

[1]Associate member.

N	number of species
N_R	number of reactions
n	coordinate normal to the streamline
n_a, n_b	temperature exponents in the rate expression
p	static pressure
q	magnitude of velocity
R	gas constant
R_o	universal gas constant
s	streamline coordinate
T	static temperature
u	x component of velocity
V	any dependent variable
W_k	molecular weight
x,y	Cartesian coordinates
Y_k	molar concentration
$\dot{Y}_k$	rate of change of Y_k
$Z_{\ell,k}$	third body efficiency
α_k	mass fraction
γ_k	α_k/W_k
δ_k^*	characteristic length in the viscosity model
θ	flow angle
μ	effective turbulent viscosity
ν,ν'	stoichiometry coefficients
ρ	density
ψ	stream function
ω	net specie exchange rate

Subscripts:

A,B,C,D	different chemical species
a,b	respectively, forward and reverse reaction
i,j	grid points (Fig. 8)
k	specie number
ℓ	reaction number

M third body

∞ main stream

INTRODUCTION

Recently, analytical modeling of the diffusive combustion and ignition processes (1-3) have received attention due to their application to the design of the supersonic-combustion ram-jet engine.

While most of previous investigations were concerned with axisymmetric configuration, this paper considers a two-dimensional configuration in which hydrogen is injected from a rearward facing step in the direction parallel to the main stream.

In the literature dealing with similar reactive-flow problems, it is usually assumed in the analysis that the chemical source terms may be modeled by expressing the reaction rates in terms of time-average quantities. For example, this assumption was made in reference (1) where individual combustion reactions were considered, and in references (2,3) where global expressions were used to model chemical reaction. It is also usually assumed that there is no direct influence of chemical reaction on the turbulent transport mechanism, i.e., that the turbulent transport model derived from a similar but nonreactive flow field applies. Some degree of success in predicting experimental data has been achieved (1-3) by using these assumptions.

The present study provides an additional test for these assumptions by comparing the experimental results with predictions.

The existing experimental information on reactive flows is mostly related to the axisymmetric free-jet geometry so that presented experimental results extend the range of available experimental data.

The experimental conditions in the main stream corresponded to Mach number 2.44, static temperature 1270 K, and static pressure approximately equal to one atmosphere. Conditions in the hydrogen jet corresponded to sonic velocity, room total temperature and static pressure equal to that in the main stream.

EXPERIMENT

Test Section

The test section which was used in the experiment is the same as in reference (4); it is illustrated in Fig. 1. For the OH absorption measurement, the downstream windows were replaced with brass plates containing a line of 0.32 cm diameter holes, thus eliminating the windows as a source of beam attenuation. Two sets of plates were fabricated, enabling measurements to be made on 0.32 cm centers across the stream, 22.8 cm downstream of the injection step. A more detailed description of the test hardware is presented in reference (4).

Optical System

The optical technique used to determine OH concentration and temperature in this study has been developed and used in references (5-7). This method relies on absorption of the narrow lines emitted from a hydroxyl radical source by broader lines in the combustion gas.

Figure 2 illustrates the arrangement of the optical system. The OH line spectrum source was a water-cooled, end-view capillary discharge tube (6,7). The emission from the source was chopped and focused on the test section centerline with a quartz lens. The beam emerging from the other side of the test section was reflected by a spherical mirror to a focus on the entrance slit of 1/2 meter grating monochrometer which was used in the second order, thus pro-

viding a good separation of the spectral lines of interest. The spectral lines were in the 0-0 band starting around 0.307 μm. The line intensity was measured by a photomultiplier located at the exit slit. The photomultiplier output was amplified with a lock-in amplifier and the signal recorded on an x-y recorder.

Procedure

The high-temperature gas stream was produced by burning a hydrogen-nitrogen gas mixture with liquid oxygen at high pressure. The oxygen content of the products was about 21% by volume. The Mach number in the gas stream was 2.44, the static temperature 1270 K, and static pressure about atmospheric. Hydrogen was injected at sonic velocity, room total temperature, and approximately atmospheric static pressure.

Because of the use of heat absorbing hardware, the run times were limited to about 3 sec. In order to determine the temperature, absorption measurements for a number of different spectral lines are required. It was necessary, therefore, to duplicate the same run conditions a large number of times, changing the monochrometer setting between runs. A reading of emission line intensity with no absorbing gas present was recorded before and after each run. If the pre- and post-run levels were not the same, within about 2 percent, the data from the particular run were discarded. For consistency, the recording trace was always read at the same point relative to the end of the run.

After a series of runs was completed at one location, the optical system was realigned through the next hole and another series of runs initiated.

Overall, measurements were taken at 9 different locations across the stream, ranging from 0.6 to 6.0 cm from the wall, all at the axial location 22.8 cm downstream of the hydrogen injection step.

A brief description of the data analysis procedure is given in Appendix A.

ANALYSIS

The Equations

It is customary in the numerical solution of jet mixing problems to replace the normal coordinate y with the stream function ψ by using the following transformation.

$$\frac{\partial \psi}{\partial y} = \rho u \tag{1}$$

For the wall-jet problem this system becomes less suitable, because at the wall, the flow rate approaches zero and for the constant increment $\Delta\psi$, Δy becomes very large. This is just the opposite of the desired variation of Δy. However, in the streamline coordinate system (s,n) the boundary-layer equations are as simple as in the (x,ψ) system and at the wall $\Delta n = \Delta y$. It is noted that in the numerical procedure Δn must be allowed to vary, which necessitates the formulation of the problem for a nonuniform grid. However, this does not complicate the solution since in the numerical calculation of the boundary-layer, the use of nonuniform grid is necessary for obtaining accuracy and convergence of the solution (8-10).

Assuming that turbulent Prandtl and Lewis number are unity, the time average boundary layer equations written in terms of effective turbulent viscosity μ are,

$$\rho q \frac{\partial q}{\partial s} = \frac{\partial}{\partial n}\left(\mu \frac{\partial q}{\partial n}\right) \tag{2}$$

$$\rho q \frac{\partial H}{\partial s} = \frac{\partial}{\partial n}\left(\mu \frac{\partial H}{\partial n}\right) \tag{3}$$

$$\rho q \frac{\partial Y_k}{\partial s} = \frac{\partial}{\partial n}\left(\mu \frac{\partial \alpha_k}{\partial n}\right) + W_k \dot{Y}_k \tag{4}$$

$$\frac{\partial(\rho q)}{\partial s} + \rho q \frac{\partial \theta}{\partial n} = 0 \tag{5}$$

and the equation of state is

$$p = \rho T R_o \sum_1^N \frac{\alpha_k}{W_k} \tag{6}$$

The assumption that Prandtl and Lewis numbers are equal to one has been made because the equations are much simpler in this case and it appears that there is no concensus in the literature as to their values.

The Effective Viscosity

The turbulent viscosity formulation is as in reference (4). It is essentially based on the Herring-Mellor (11) kinematic eddy viscosity model developed for a turbulent boundary layer. The modification of the model is in the near region where the free-shear layer has not yet merged with the developing wall boundary-layer. In this region, the kinematic viscosity in the free-shear layer - analogous to the viscosity in the outer portion of the boundary layer (11) - is taken to be proportional to length δ_k^* given by

$$\delta_k^* = \int_{y_3}^{y_4} (q_\infty - q)/q_\infty \, dy$$

where y_3 and y_4 correspond to free-shear layer boundaries, Fig. 3, determined so that the deviation from uniform flow on either side is about 0.1 percent. All constants in the model are as determined originally in reference (11).

Using this model in reference (4) good agreement between experimental and computed composition profiles was obtained for the case of no reaction. It is noted, however, that the model has not been tested by applying it to other experimental data.

Chemical Species Production Terms

All the reactions considered in the analysis could either be represented by a bimolecular reaction

$$\nu_A(\ell)A + \nu_B(\ell)B \rightleftarrows \nu_C'(\ell)C + \nu_D'(\ell)D \tag{7}$$

or a three-body recombination reaction

$$\nu_A(\ell)A + M \rightleftarrows \nu_B'(\ell)B + \nu_C'(\ell)C + M \tag{8}$$

where $\nu_i(\ell)$, i = A,B,C and D are the stoichiometric coefficients for reaction number ℓ, and M is the third body. Then, for example, for specie A, the chemical production rate is given by

$$\dot{Y}_A = \sum_1^{N_R} [\nu_A'(\ell) - \nu_A(\ell)]\omega_\ell \tag{9}$$

where

$$\omega_\ell = f_a(\ell) Y_A^{\nu_A(\ell)} Y_B^{\nu_B(\ell)} - f_b(\ell) Y_C^{\nu'_C(\ell)} Y_D^{\nu'_D(\ell)}$$

for reaction (7) and

$$\omega_\ell = f_a(\ell) Y_A^{\nu_A(\ell)} Y_M(\ell) - f_b(\ell) Y_B^{\nu'_B(\ell)} Y_C^{\nu'_C(\ell)} Y_M(\ell)$$

for reaction (8). The molar concentration $Y_M(\ell)$ depends on the assigned third body efficiencies $Z_{\ell,k}$, $k = 1, \ldots, N$

$$Y_M(\ell) = \sum_{k=1}^{N} Z_{\ell,k} Y_k \tag{10}$$

The temperature dependence for the forward reaction rate f_a, for example, is given by

$$f_a(\ell) = \bar{A}_a(\ell) T^{n_a(\ell)} \exp[-E_a(\ell)/RT] \tag{11}$$

Eighteen chemical reactions and nine chemical species were considered in the analysis. The reaction scheme and the rate information are essentially the same as presented in reference (12).

Numerical Methods

The system of equations (2) to (6), together with appropriate equations for the production of species is a quasi-linear system of parabolic equations. Since the chemical specie production terms do not involve derivatives, they could be computed from values of dependent variables calculated from the previous integration step. However, because of the well known difficulty in integration of the one-dimensional flow problems involving chemical kinetics equations, special techniques were used in the past to evaluate the effect of chemical production terms.

In reference (1) diffusion and reaction steps were solved independently and then the respective solutions were superimposed at each integration step. A special integration technique which had been developed for the one-dimensional problem was applied for the reaction step. This technique is based on linearization of the chemical production terms and the solution of the resulting set of linear differential equations by the use of parabolic fits for the specie concentrations. For the solution of the diffusive step, the explicit difference scheme was applied.

Because of the presence of the boundary layer in the wall-jet problem considered in this report, the integration of the diffusion step by the explicit method becomes impractical and so an implicit integration method is used. For the integration of the reaction step, the method of Lomax and Bailey (13) has been selected.

These two steps and the coupling scheme are discussed more fully in Appendix B.

The Initial Conditions

The initial composition in the main stream was calculated by using the general one-dimensional computer program of Bittker and Scullin (12). The calculation was started in the gas generator and terminated at the test sec-

tion entrance. In addition to the chemical reactions involving hydrogen-oxygen species, several reactions involving the NO radical were also included in the calculation. However, the inclusion of these reactions had no effect on the ignition delay on the one-dimensional basis (4) and, therefore, they were omitted in subsequent two-dimensional calculations.

The calculated initial composition in mole-fractions is $[H_2] = 0.193\times10^{-4}$, $[O_2] = 0.208253$, $[H_2O] = 0.3410570$, $[H] = 0.8\times10^{-6}$, $[O] = 0.29\times10^{-4}$, $[OH] = 0.3419\times10^{-3}$, $[HO_2] = 0.48\times10^{-5}$, $[H_2O_2] = 0.27\times10^{-5}$, and $[N_2] = 0.4502913$.

The calculated static temperature in the main stream proved to be somewhat higher than the experimental value. This discrepancy is believed to be due to the heat transfer effects which have not been included in the computation. Since it was essential to reproduce the static temperature correctly, the composition of the reactants in the gas generator chamber was adjusted by reducing the hydrogen content slightly until the resulting static temperature was sufficiently close to the experimental value.

The initial velocity and temperature distribution determined on the basis of measurements are as presented in reference (4).

In the experiment, largely because of the boundary-layer build-up on the test section walls, a small change in the mainstream flow variables was noticed between test section entrance and exit. In the analysis, this change was assumed to take place linearly. The equations for the main stream velocity, static temperature, and static pressure are:

$$q_\infty = 1791 - (x/35.6)128.8 \text{ m/s} \tag{12}$$

$$T_\infty = 1259 + (x/35.6)76.9 \text{ K} \tag{13}$$

$$P_\infty = 9.24\times10^4 + (x/35.6)2.48\times10^4 \text{ N/m}^2 \tag{14}$$

COMPARISON OF ANALYSIS AND EXPERIMENT

Ignition Distance

The measured ignition distance determined from the boundary of the luminous zone was on the average about 15 cm, whereas the calculated ignition distance determined on the basis of a 5 percent rise in static temperature above the mainstream value was 16.5 cm.

The agreement between measured and calculated values is satisfactory, particularly in view of the large temperature difference between the hydrogen jet and the main stream.

Comparison of Predicted Profiles with Optical Measurements

The static temperature profiles at $x = 22.8$ cm are presented in Fig. 4, while the OH mole fractions are presented in Fig. 5. The calculated profiles are presented for two sets of main-stream composition. One set corresponds to the calculated composition. In the other, the OH mole fraction is adjusted to correspond to the measured main-stream value. The mole fraction of other radicals were also adjusted in the same proportion.

Good agreement is noted in Fig. 4 between predicted and experimental values of maximum temperature, when the prediction is based on experimental value of OH in the main stream. However, predicted temperature profile is considerably narrower. A much more gradual approach to the main-stream temperature is noted in the experimental profile.

For the case of calculated main-stream composition the predicted maximum

temperature is about 200 K higher than the experimental. However, the average width of the calculated temperature profile now more closely corresponds to the experimental value.

The OH profiles in Fig. 5 indicate considerable differences between theoretical and experimental values. The magnitude of the deviation appears to be proportional to the OH level which is the opposite of the trend observed in Fig. 4 for temperature profiles. Qualitatively, this could be explained by the way these two measurements are influenced by the nonuniformities across the optical path length introduced by turbulence and by the presence of the test-section side boundary-layers. The hydroxyl radical distribution is averaged evenly, independently of the magnitude, whereas, in the case of temperature, the indicated value more closely corresponds to the maximum across the path length.

The optical path length used in the data reduction has not been corrected for the presence of the side boundary-layers. Because of associated effects due to test-section corners, the correction is probably more significant in the region close to the wall (small y). In the main stream, reasonable agreement is noted between experimental and predicted OH mole fractions.

To illustrate to what extent the hydroxyl radical concentration varies in the x direction in this region, also plotted in Fig. 5 is the calculated profile of $x = 20.1$ cm. It is seen that in a distance of less than 3 cm the OH mole fraction varies by more than an order of magnitude.

Comparison of Predicted Profiles with Probe Measurements of Ref. (4)

In reference (4) the composition and the flow fields derived from probe measurements at $x = 35.6$ cm were compared with corresponding predicted profiles which were computed by assuming that combustion reactions are in chemical equilibrium. The composition profiles from reference (4) are reproduced in Fig. 6. It can be seen from Fig. 7 that the agreement between theory and experiment is now better and that, therefore, as anticipated, some of the observed shift of the calculated profiles in relation to the experimental in Fig. 6 is mainly due to the equilibrium assumption.

In Fig. 7, the most noticeable departures of computed profiles in relation to experimental profiles are: (1) lower mole fractions of hydrogen and higher mole fractions of water vapor in the region where $y < 2$ cm, and (2) more gradual profile slopes in the region where $y > 2$ cm. The latter indicates that the assumed mixing rate in the outer portion of the boundary layer is too high. It is also possible that a better prediction of the experimental results could be obtained in the region where $y < 2$ cm by assuming a lower mixing rate in this region, because this assumption would cause an increase in hydrogen concentration and a reduction in water-vapor concentration. This is evidenced by comparing Figs. 6 and 7. The thickness of the mixing/boundary-layer region in the predicted profile in Fig. 6 is smaller than in Fig. 7. Because viscosity is proportional to this thickness, it follows that viscosity is also smaller, and it can be seen that the hydrogen mole fraction at the wall is predicted better in Fig. 6.

Taking into account the results of the previous section and of the fact that the ignition distance is fairly well predicted, the overall effect concerning the rate of reaction is that it is fairly well modeled up to the ignition point and that it is somewhat overpredicted downstream of it.

Comparison was also made between predicted and experimental profiles of total temperature and the Mach number. The total temperatures agreed fairly well and markedly better than in reference (4). However, significant differences, particularly in the region close to the wall were noted in the case of Mach numbers. The difference, it is believed, arises because of excessive flow deceleration in the test section caused by boundary-layer effects. A similar conclusion was made in reference (4) comparing Mach numbers for the

case of no reaction.

CONCLUSION

For the wall-jet configuration, the use of the time-average concentration and the molecular reaction rate expressions together with a kinematic eddy-viscosity representation of the turbulent transport phenomena results in (1) a reasonably accurate prediction of the ignition distance, (2) a fair prediction of the magnitude and the relative position of the peak static temperature in the early stages of the flame development, provided that the hydroxyl radical level in the main stream is based on the experimental value, and (3) a fair prediction of the stable specie distribution in the diffusion-reaction zone.

The departure of theoretical predictions from experimental results indicates that the assumed turbulent transport model causes the rate of mixing in the outer portion of the mixing-boundary layer to be too high and that the resulting theoretical rate of reaction is somewhat over-estimated downstream of the ignition point.

REFERENCES

1 Ferri, A., Moretti, G., and Slutsky, S., "Mixing Processes in Supersonic Combustion," Journal of Society of Industrial and Applied Mathematics, Vol. 13, 1965, pp. 229-258.

2 Cohen, L. S., and Guile, R. N., "Measurements in Freejet Mixing/Combustion Flows," AIAA Journal, Vol. 8, No. 6, 1970, pp. 1053-1061.

3 Bray, K. N. C., and Fletcher, R. S., "Pilot Ignition of Cold Supersonic Flows," AIAA Journal, Vol. 10, No. 1, 1972, pp. 72-79.

4 Burrows, M. C., and Kurkov, A. P., "An Analytical and Experimental Study of Supersonic Combustion of Hydrogen in Vitiated Air Stream," AIAA Journal, Vol. 11, No. 9, 1973, pp. 1217-1218, see also NASA TM X-2828.

5 Kaskan, W. E., "Hydroxyl Concentrations in Rich Hydrogen-Air Flames Held on Porous Burners," Combustion and Flame, Vol. 2, No. 3, 1958, pp. 229-243.

6 Lezberg, E. A., and Buchele, D. R., "Some Optical Techniques for Temperature and Concentration Measurements of Combustion in Supersonic Streams," NASA TN D-2441, 1964.

7 Lezberg, E. A., Rose, C. M., and Friedman, R., "Comparisons of Experimental Hydroxyl Radical Profiles with Kinetic Calculations in a Supersonic Nozzle," NASA TN D-2883, 1965.

8 Harris, J. E., "Numerical Solution of the Equations for Compressible Laminar, Transitional and Turbulent Boundary Layers and Comparisons with Experimental Data," NASA TR R-368.

9 Cebeci, T., and Smith, A. M. O., "A Finite-Difference Method for Calculating Compressible Laminar and Turbulent Boundary Layers," Journal of Basic Engineering, Trans. ASME, Series D, Vol. 92, No. 3, Sept. 1970, pp. 523-535.

10 Bushnell, D. M., and Beckwith, I. E., "Calculation of Non-Equilibrium Hypersonic Turbulent Boundary Layers and Comparisons with Experimental Data," AIAA Journal, Vol. 8, No. 8, 1970, pp. 1462-1469.

11 Herring, H. J., and Mellor, G. L., "A Method of Calculating Compressible Turbulent Boundary Layers," NASA CR-1144, 1968.

12 Bittker, D. A., and Scullin, V. J., "General Chemical Kinetics Com-

puter Program for Static and Flow Reactions with Application to Combustion and Shock-Tube Kinetics," NASA TN D-6586, 1972.

13 Lomax, H., and Bailey, H. E., "A Critical Analysis of Various Numerical Integration Methods for Computing the Flow of a Gas in Chemical Nonequilibrium," NASA TN D-4109, 1967.

14 Learner, R. C. M., "The Influence of Vibration-Rotation Interaction on Intensities of the Electronic Spectra of Diatomic Molecules. I. The Hydroxyl Radical," Proceedings of the Royal Society (London), Ser. A., Vol. 269, No. 1338, 1962, pp. 311-326.

15 McDonald, H., "An Assessment of Certain Procedures for Computing the Compressible Turbulent Boundary Layer Development," Compressible Turbulent Boundary Layers, NASA SP-216, 1969, pp. 181-200.

16 Moretti, G., "A New Technique for the Numerical Analysis of Nonequilibrium Flows," AIAA Journal, Vol. 3, No. 2, 1965, pp. 223-229.

APPENDIX A

The absorption coefficient, $\bar{\alpha}$, is given in terms of the path length, L, the measured line intensity with no absorber present, I_o, and the line intensity after passing through the absorbing gas, I,

$$\bar{\alpha} = \ln(I_o/I)/L \tag{15}$$

On assuming rotational equilibrium, temperature is determined from the Boltzmann plot, an example of which is illustrated in Fig. 8. The ordinate in this figure is the natural logarithm of the ratio of absorption coefficient to the product of the relative transition probability, A_k, and a correction factor for vibrational-rotational interaction, $T_{J'J''}$ (14). The abscissa is the wave number of the rotational level, ω_k, divided by the Boltzmann constant k and multiplied by the product of Planck's constant h, and the speed of light, c. The slope of the line in Fig. 8 is the inverse of the temperature.

The number density of the OH radicals, N_{OH}, is given as:

$$N_{OH} = 2.4\times10^{12}\,\frac{Q_R Q_V b_D \bar{\alpha}}{F A_k T_{J'J''}}\exp\left(\frac{hc\omega_k}{kT}\right) \tag{16}$$

where Q_R and Q_V are, respectively, rotational and vibrational partition functions; b_D is the Doppler half-width of the observed spectral line; and F is a constant taken from reference (6).

APPENDIX B

Integration of the Diffusion Step

In the absence of reaction the problem reduces to the solution of the turbulent boundary-layer coupled with the jet-mixing flow. The differenced form of the boundary-layer equations (2) to (4) for the mesh defined in Fig. 9 is given by

$$(\rho q)_{i,j}\,\frac{V_{i+1,j} - V_{i,j}}{\Delta s_{i,j}} = \frac{1}{\Delta n_{i,j-1/2}}\left(\mu_{i,j+1/2}\,\frac{V_{i+1,j+1} - V_{i+1,j}}{\Delta n_j} - \mu_{i,j-1/2}\,\frac{V_{i+1,j} - V_{i+1,j-1}}{\Delta n_{j-1}}\right) \tag{17}$$

where V stands for either q, H, or α_k.

The continuity equation (5) is integrated by centering θ halfway between the grid points,

$$\frac{(\rho q)_{i+1,j} - (\rho q)_{i,j}}{\Delta s_{i,j}} + (\rho q)_{i,j} \frac{\theta_{i+1,j+1/2} - \theta_{i+1,j-1/2}}{\Delta n_{i,j-1/2}} = 0 \tag{18}$$

Once θ is known new grid spacings can be computed by using simple geometrical relations. For example, $\Delta n_{i+1,j-1/2}$ is given by

$$\Delta n_{i+1,j-1/2} = \Delta n_{i,j-1/2} + \Delta s_{i,j}(\theta_{i,j+1/2} - \theta_{i,j-1/2}) \tag{19}$$

Because the difference equations are implicit, it is noted that the nonuniform grid spacing does not introduce any stability problems.

Because of large variation in viscosity, it was found necessary to vary the initial Δn spacing. This was done so that approximately

$$(\rho q/\mu)\Delta n^2 \sim \text{constant}$$

without allowing an excessively large rate of increase of Δn away from the wall. In practice, following this guideline usually resulted in a mesh with several constant Δn spacings next to the wall followed by a section where Δn increased by a factor of 1.5 to 2 after which Δn was again constant. Total number of points in the normal direction was typically about 30.

For the jet-mixing problem, the results obtained using this integration scheme were in agreement with results obtained by using a program which employed the stream function transformation (1) and a uniform grid spacing.

In the case of a turbulent boundary layer, the present program predicted somewhat lower values for the displacement thickness in comparison with the calculation of Herring and Mellor (11). The normalized velocity profiles, however, agreed very well. In this regard, it may be noted that slight discrepancies in the prediction of turbulent boundary layers which apparently result from the use of different numerical schemes have been observed in the past (15).

The Reaction Step and the Coupling Scheme

Since the effects of the chemical reaction are evaluated independently of the diffusion process, equations (4) and (3) reduce to

$$\frac{d\gamma_k}{ds} = (1/\rho q)\dot{Y}_k(T,\rho,\gamma_1, \ldots,\gamma_N), \quad k = 1, \ldots,N \tag{20}$$

$$\frac{dT}{ds}\sum_1^N \gamma_k W_k (C_p)_k + \sum_1^N W_k h_k \frac{d\gamma_k}{ds} = 0 \tag{21}$$

where

$$\gamma_k = \alpha_k/W_k$$

The system of equations is completed with

$$R_o T \frac{d\rho}{ds} \sum_1^N \gamma_k + \rho R_o \frac{dT}{ds} \sum_1^N \gamma_k + \rho R_o T \sum_1^N \frac{d\gamma_k}{ds} = 0 \qquad (22)$$

which is obtained from equation (6) by differentiation.

The integration method is based on an implicit difference scheme (13) which is applied to the linearized system of equations. Linearization is carried out uniformly with respect to all the dependent variables $\gamma_1, \ldots, \gamma_N$, T, and ρ. The derivatives are replaced using the simple formula

$$V_{i+1} = V_i + (1/2)\Delta s\left[\left(\frac{dV}{ds}\right)_{i+1} + \left(\frac{dV}{ds}\right)_i\right] \qquad (23)$$

where V represents any dependent variable. Substitution of $(dV/ds)_{i+1}$ and $(dV/ds)_i$ in (23) is performed by using equations (20) to (22) upon linearization. It is noted that information at only one point (i) is needed in order to compute variables for a new point (i + 1).

The computation scheme differs from that in reference (13) in that the coefficients in the linearized equations are computed from derived expressions rather than by employing numerical differentiation. This improves the efficiency of computation since the number of times such functions as those describing the rate of reactions are evaluated can be significantly reduced. The linearization has been carried out for a general case of arbitrary number of reactions.

On the one-dimensional basis, the results obtained by this method were in good agreement with Morretti's solution (16) which is based on the exact solution of the linearized system of differential equations.

The coupling of diffusion and reaction steps can be accomplished in several ways. In the present program it is carried out by first solving the diffusion equations and then the reaction equations. The values of $\gamma_1, \ldots, \gamma_N$, ρ, and T calculated at the end of diffusion step are used as initial values for the reaction step. The spacing Δs is controlled by the reaction step.

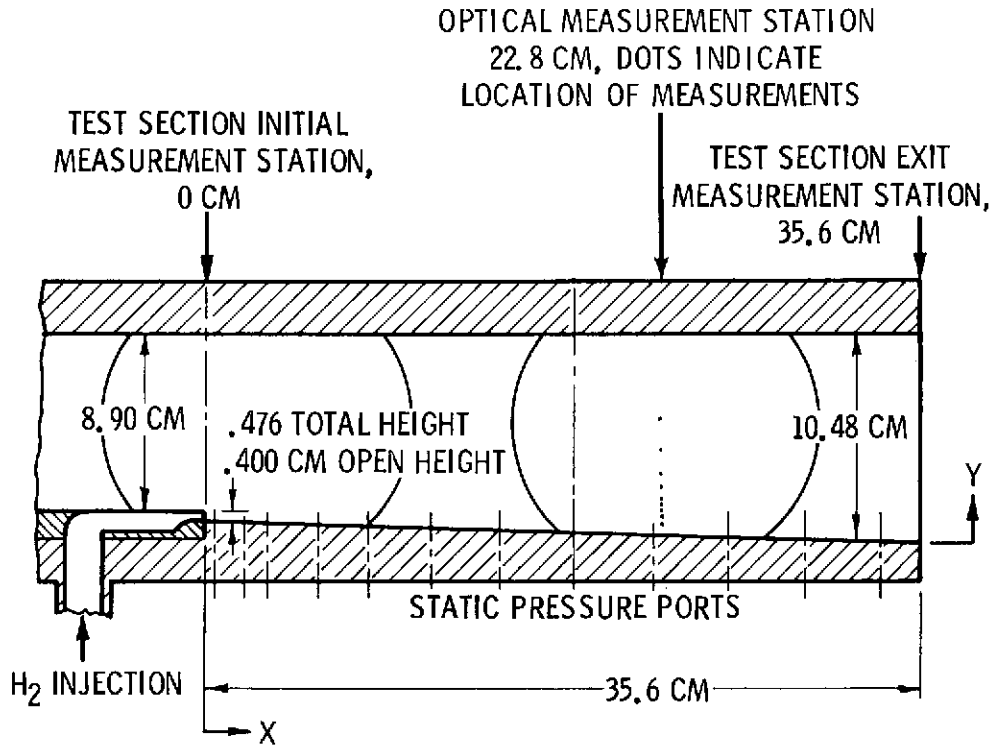

Figure 1. - The test section.

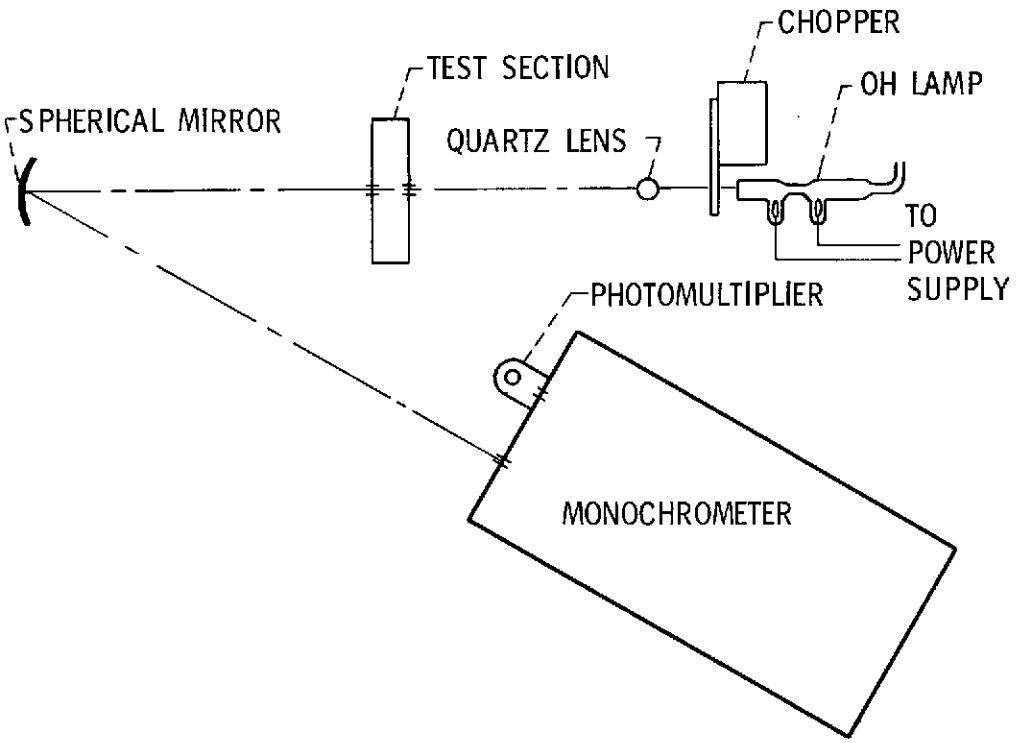

Figure 2. - Schematic of optical system used to measure temperature and OH concentration by UV absorption.

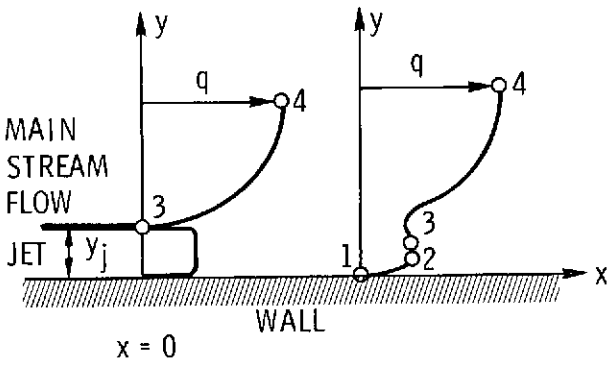

Figure 3. - Schematic of the near flow-field.

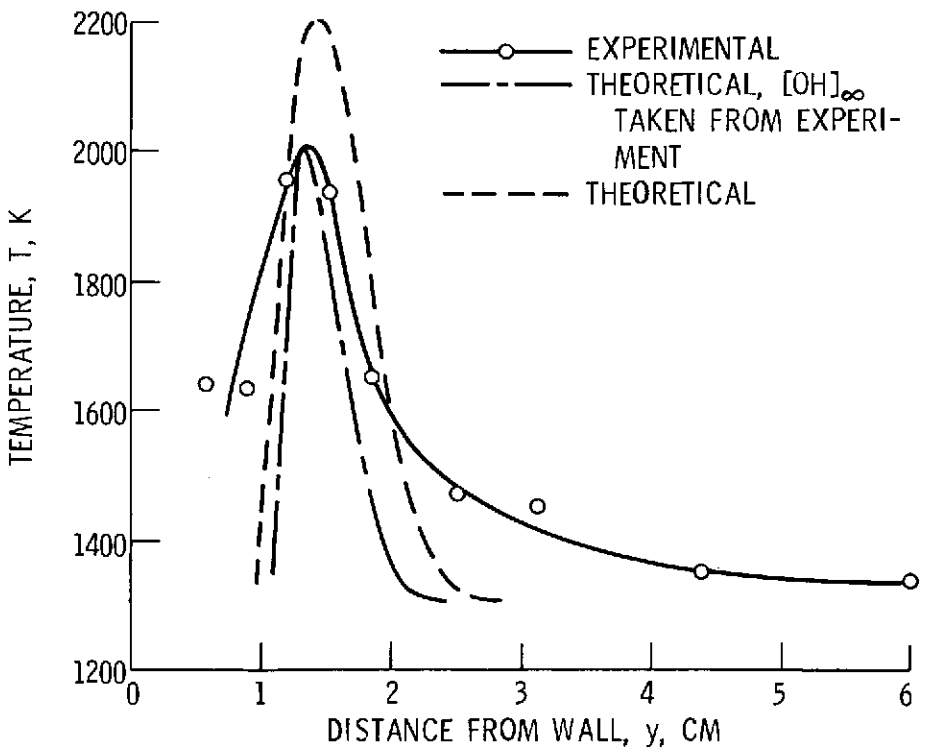

Figure 4. - Temperature profiles at x = 22.8 cm.

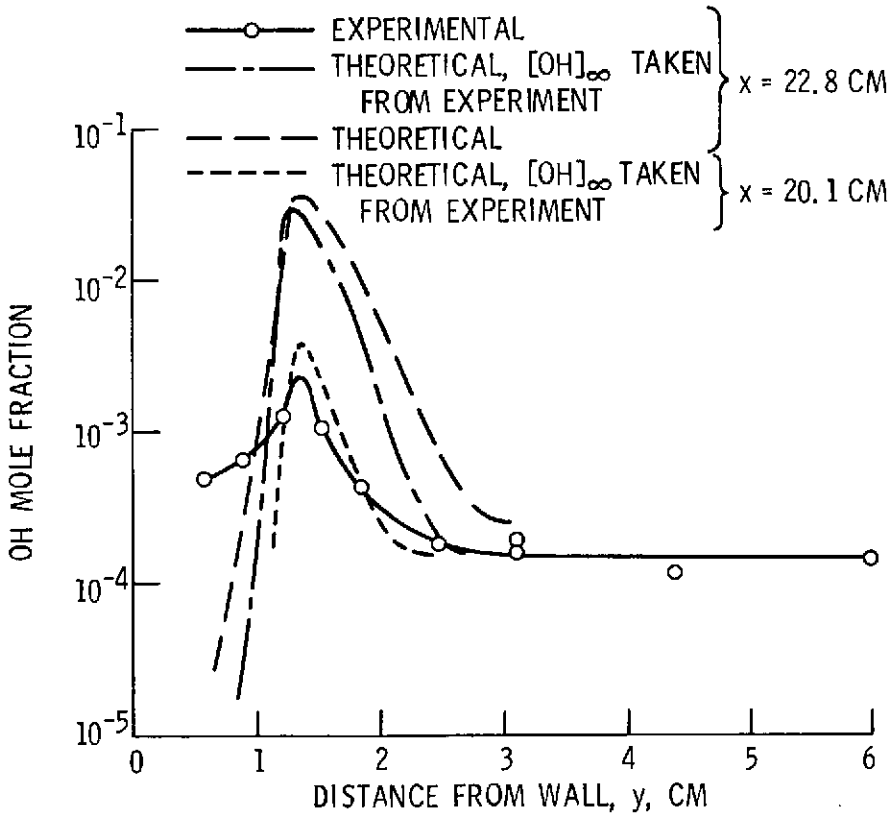

Figure 5. - Hydroxyl radical profiles.

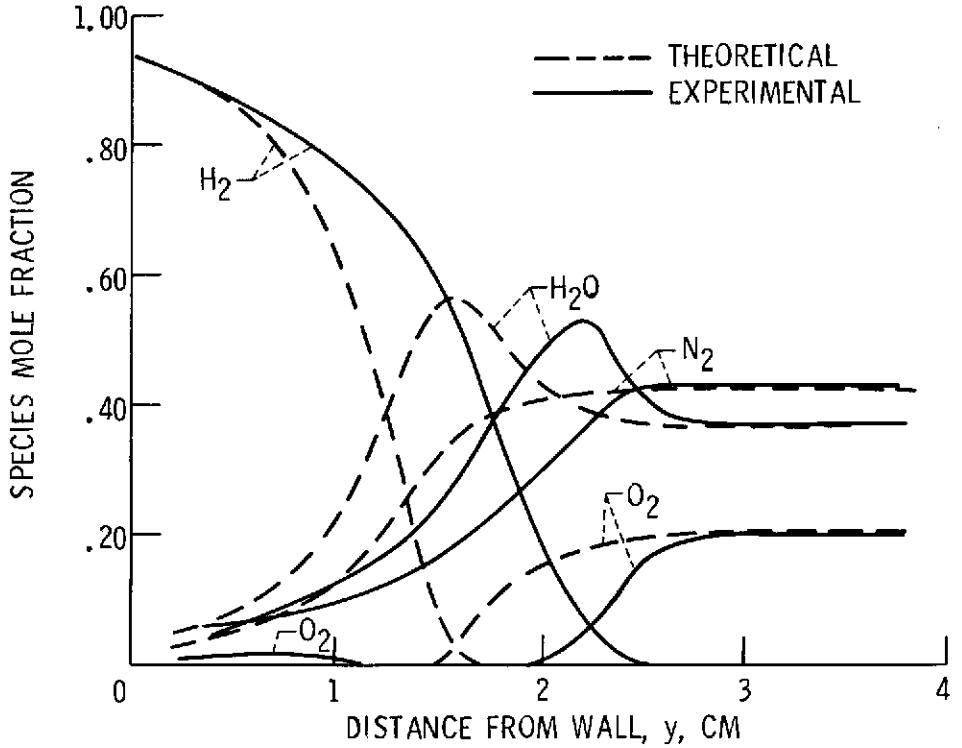

Figure 6. - Theoretical and experimental composition profiles. Equilibrium chemistry. (From reference [4])

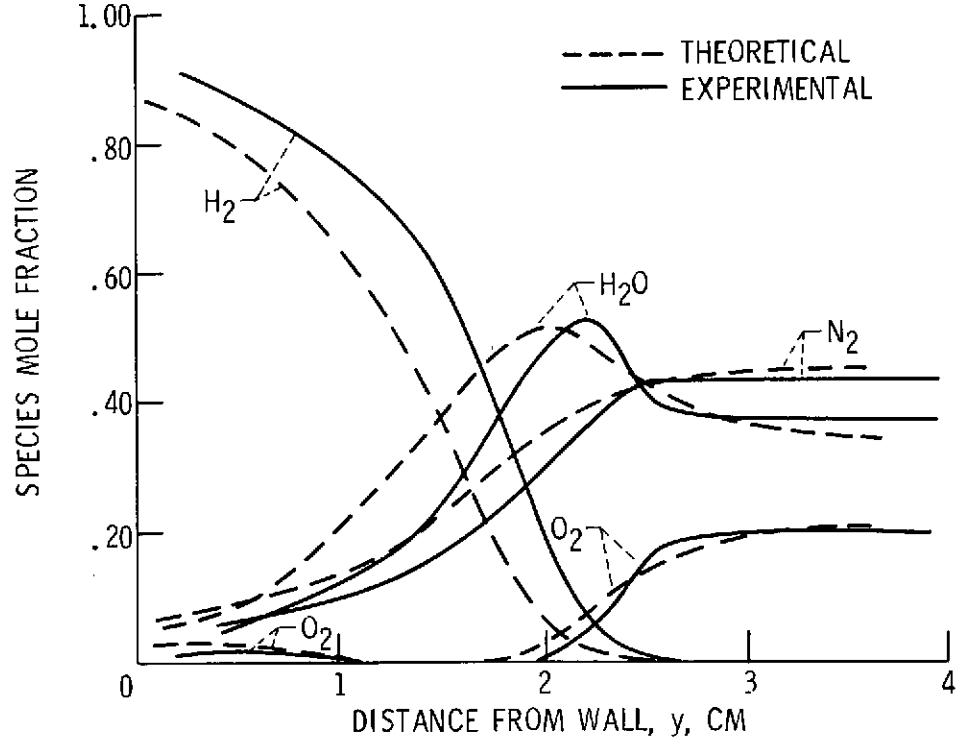

Figure 7. - Theoretical and experimental composition profiles. Nonequilibrium chemistry.

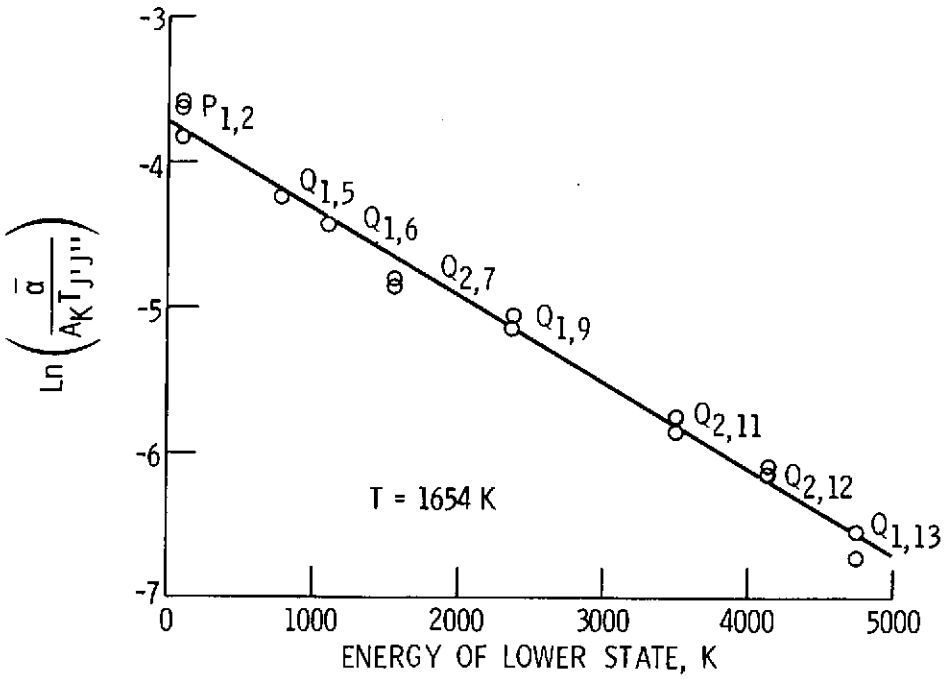

Figure 8. - Boltzmann plot of OH line absorption measurements 1.85 cm from wall. Symbols in the plot denote particular rotational lines.

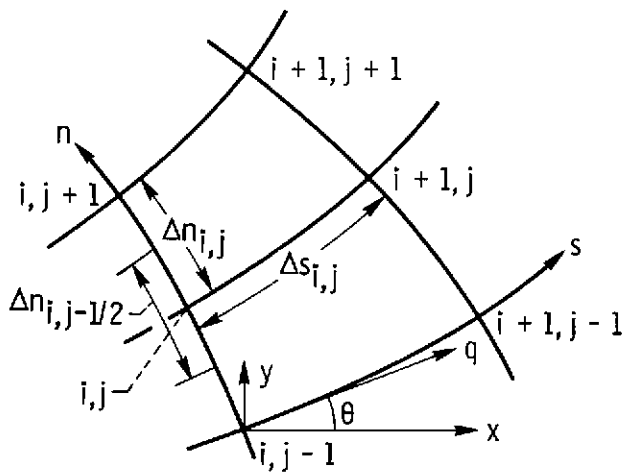

Figure 9. - Definition of grid points and spacings.